



Microstructural characteristics and cellular responses of a potential germanium bearing titanium binary alloy for dental applications

Takaaki Ueno^a, Chiung-Fang Huang^{b,c,1}, Kayoko Yamamoto^a, Wen-Chien Lan^d, Shih-Chi Lee^e, Bai-Hung Huang^{f,g,h}, Yung-Chieh Cho^{g,i}, Christopher J. Walinski^j, Muhammad Ruslin^k, Chen-Han Lee^{i,l}, Keng-Liang Ou^{a,d,g,l,m,n,*}, Hiroyuki Nakano^{a,l,*}

^a Division of Medicine for Function and Morphology of Sensor Organs, Department of Dentistry and Oral Surgery, Osaka Medical College, Osaka 569-8686, Japan

^b School of Dental Technology, Taipei Medical University, Taipei 110, Taiwan

^c Division of Family and Operative Dentistry, Department of Dentistry, Taipei Medical University Hospital, Taipei 110, Taiwan

^d Department of Oral Hygiene Care, Ching Kuo Institute of Management and Health, Keelung 203, Taiwan

^e Industrial Technology Master Program in Medical Devices, College of Oral Medicine, Taipei Medical University, Taipei 110, Taiwan

^f Graduate Institute of Dental Science, College of Dentistry, China Medical University, Taichung 404, Taiwan

^g Biomedical Technology R & D Center, China Medical University, Taichung 404, Taiwan

^h Implant Academy of Minimally Invasive Dentistry, Taipei 106, Taiwan

ⁱ School of Dentistry, College of Oral Medicine, Taipei Medical University, Taipei 110, Taiwan

^j Department of Dental Medicine, Touro College of Dental Medicine, Hawthorne, NY 10532, USA

^k Department of Oral and Maxillofacial Surgery, Faculty of Dentistry, Hasanuddin University, Makassar 90245, Indonesia

^l Taiwan Society of Blood Biomaterials, New Taipei City 221, Taiwan

^m Department of Dentistry, Taipei Medical University-Shuang Ho Hospital, New Taipei City 235, Taiwan

ⁿ 3D Global Biotech Inc. (Spin-off Company from Taipei Medical University), New Taipei City 221, Taiwan

ARTICLE INFO

Keywords:

Ti–5Ge alloy
Heat-treatment
Microhardness
Wettability
Biocompatibility

ABSTRACT

In the present study, the as-cast Ti–5Ge (wt%) (AS-TG) alloy was used to evaluate the effect of solution heat-treatment temperatures on the microstructure, phase transformation, and biocompatibility. The AS-TG specimen was subjected to different solution heat-treatment temperatures from 700 °C to 1000 °C for 30 min, and then characterized using a field-emission scanning electron microscopy, X-ray diffractometry, transmission electron microscopy, Vickers microhardness, and contact angle goniometry. The in vitro biocompatibility levels of specimens were assessed through 3-[4,5-dimethylthiazol-2-yl]-2,5-diphenyltetrazolium bromide (MTT) assay with osteoblast-like (MG-63) and fibroblast (NIH-3T3) cell lines. Analytical results indicated that the grain size of the AS-TG specimen increased with an increasing treatment temperature. Needle-like structures were formed in the matrix when the temperature was above 900 °C. The examination of transmission electron microscopy confirmed that the AS-TG specimen was in the α phase, while α and α' phases co-existed in the specimens as temperature was above 900 °C, which also exhibited higher microhardness and lower contact angle. None of the investigated specimens showed a deleterious effect on MG-63 or NIH-3T3 cells, and were at the same level as commercial pure Ti, indicating good biocompatibility. Moreover, both MG-63 and NIH-3T3 cells presented excellent cell adhesion and proliferation abilities when temperature was 1000 °C. Thus, the AS-TG alloy heat-treated at 1000 °C possessed the greatest microhardness and wettability as well as highest cell viability, and could be considered as a potential biomaterial for dental applications.

1. Introduction

The dramatic increase in the average age of the world population has

led to increased demand for metallic biomaterials for failed hard-tissue reconstruction [1]. Commercially available pure titanium (cp-Ti) has been used in orthopedic and dental implants since its anti-corrosion

* Corresponding authors at: Division of Medicine for Function and Morphology of Sensor Organs, Department of Dentistry and Oral Surgery, Osaka Medical College, Osaka 569-8686, Japan.

E-mail addresses: klou@tmu.edu.tw (K.-L. Ou), hiroyuki.nakano@ompu.ac.jp (H. Nakano).

¹ Co-first author: Chiung-Fang Huang.

<https://doi.org/10.1016/j.matchar.2021.111353>

Received 6 May 2021; Received in revised form 22 July 2021; Accepted 23 July 2021

Available online 25 July 2021

1044-5803/© 2021 Elsevier Inc. All rights reserved.

performance and biocompatibility property. While, the artificial implant made by cp-Ti has certain disadvantages such as low strength and poor wear resistance [2,3]. Accordingly, different alloying elements have been tried to add to the cp-Ti for improving its disadvantages. Ti-6Al-4V alloy with extra low interstitial is currently used in various load-bearing applications for its increased mechanical strength and enhanced wear and corrosion resistance [4]. However, V and Al are recognized as high-risk elements associated with long-term health problems [5]. Therefore, it is desired to develop new metallic biomaterials by alloying Ti with several toxic- and allergy-free elements for artificial implants usage [6–9].

There are three typical metallographic phases of Ti-based alloys: the α , ($\alpha + \beta$), and β phases [10]. Attempts were made to develop metastable β -phase Ti alloys by adding non-toxic elements such as Mo, Nb, Ta, and Zr [6,11,12]. These β -type Ti alloys exhibited lower elastic moduli and enhanced corrosion resistance than two-phase ($\alpha + \beta$) Ti alloys, and were developed for their biomechanical compatibility [13]. The casting of β -type Ti alloys with the elements mentioned above was the most feasible fabrication route for biomedical devices. However, it was not easy to obtain a homogeneous composition in the casting of β -type Ti alloys because of high melting temperatures, affinities with interstitial elements, and oxidation [14]. In addition, these refractory elements alloyed to Ti are difficult to cast into defect-free materials, and thus β -type Ti alloys are restricted in dental field applications.

Recently, the addition of fusible alloying elements, such as Ga and Sn, has revealed good biocompatibility, and these were used to minimize the difficulties of casting procedures of Ti alloys [15]. Ge is known to exist in organisms widely and has been judged to be an element of relatively low risk to humans [16]. When alloyed to Ti, Ge can be used to enhance comprehensive mechanical properties [17]. Another advantage of alloying Ge to Ti is that the melting temperature of Ti (1670 °C) is lowered with an increase in the amount of Ge, thereby favoring casting procedures according to a Ti–Ge phase diagram [18]. Lin et al. [19] suggested that Ge has the potential to improve the strength of Ti alloys. They also proved no differences in the corrosion capacity between a Ti–5Ge (wt%) alloy (hereafter defined as AS-TG) and cp-Ti. As a result, the AS-TG binary alloy has great potential to be used as a dental material.

Phases and crystal structures, which can be controlled by metallurgical techniques, were proven to influence the mechanical behaviors and biocompatibility of Ti alloys [20]. It is well known that there are two metastable martensite phases, α' and α'' [21]. The α' phase exhibits a hexagonal structure, whereas the α'' phase possesses an orthorhombic structure. The altering of the amounts of alloying elements and thermal treatment can control the transformation of these two phases. As stated above, the present study was aimed to investigate the effects of different solution heat-treatment temperatures on the microstructure, phase transformation, and biocompatibility of the AS-TG binary alloy, and attempt to provide useful information for further applications in the dental field.

2. Materials and methods

2.1. Specimens preparation

The AS-TG alloy ingots were prepared from pure Ti sponge (99.9% purity) and Ge ingots (99.9% purity), which were supplied by Well-Being Enterprise Co. (New Taipei City, Taiwan), in the vacuum arc melting furnace. The melt was poured into a preheated steel mold. The specimens with $10 \times 10 \times 2 \text{ mm}^3$ dimensions were mechanically cut from the obtained ingots. The chemical compositions of the investigated AS-TG alloy were verified through a field-emission scanning electron microscopy (SEM; JEOL JSM-6500F, Japan) equipped with a wavelength dispersive spectroscopy (Oxford Instruments, UK) as shown in Table 1. The AS-TG specimens were solution heat-treated (SHT) under different temperatures of 700 °C, 800 °C, 900 °C, and 1000 °C for 30 min

Table 1

Chemical compositions of the investigated AS-TG binary alloy.

O	N	C	Ge	Ti
0.14	< 0.01	0.02	4.82	Bal.

followed by water quenching (hereafter denoted as SHT-700, SHT-800, SHT-900, and SHT-1000, respectively). In this study, the grade 4 cp-Ti with SHT at 700 °C for 30 min acted as control group for comparison.

2.2. Surface characterization

The SHT specimens, as well as the AS-TG, were sectioned, polished, and etched by a mixed solution of 3 mL HF, 2 mL HNO₃, and 95 mL H₂O for 40 s, followed by ultrasonic cleaning in acetone, distilled, ethanol, and distilled water for 15 min each. The optical microscopy (OM; Olympus BX 51, Japan) and JEOL JSM-6500F SEM with an energy dispersive spectroscopy (EDS; Oxford Instruments, UK) were used to characterize the metallurgical microstructure and chemical composition. Phase identification was performed by X-ray diffractometry (XRD; RIGAKU 2200 with Cu K α radiation, Japan) under an accelerating voltage of 40 kV and a current of 30 mA. The further phase identification and crystallinity were also carried out by a transmission electron microscopy (TEM; JEOL JEM-2100, Japan) at an accelerating voltage of 200 kV. A thin foil of TEM specimen was prepared by twin-jet electropolishing in a solution of 20% nitric acid (by volume) and 80% methanol. Vickers microhardness was measured on the specimen at a load of 100 g for 15 s using a microhardness tester (Akashi MVK-H1, Mitutoyo Corp., Japan). The hardness values for each specimen were the average of five distinct measurements. The surface wettability of specimens ($n = 5$) was assessed via the sessile drop method by the contact angle of a 2.5- μ L deionized water droplet, and was measured with a GBX digital contact angle meter (GBX Scientific LTD., France).

2.3. Biocompatibility evaluation

Osteoblast-like cell line (MG-63, ATCC CRL-1427, Taiwan) and fibroblast cell line (NIH-3T3, ATCC CRL-1658, Taiwan) were adopted to evaluate the biocompatibility of the investigated specimens. Cells were cultured in minimum essential medium containing 10% fetal bovine serum and 1% penicillin streptomycin for 24 h at 37 °C, and cells of the fourth passage were selected. In vitro cytotoxic effects were evaluated using a 3-(4,5-dimethylthiazol-2-yl)-2,5-diphenyltetrazolium bromide (MTT, Sigma-Aldrich, Taiwan) assay according to ISO 10993-5 standard. After specimens were autoclaved at 121 °C for 15 min, the cells (5×10^4 cell/mL) were seeded onto each group ($n = 6$) following ISO standards 10993-12 in a 24-well plate for 8 h, 24 h, 72 h and 120 h, and cultured at 37 °C with an atmosphere of 5% CO₂ and 95% air. The culture medium was refreshed every 2 days. At the end of each time point, the culture medium was replaced with 500 μ L of minimum essential medium mixed with 50 μ L of a yellow-colored MTT-labeled solution. After cells were incubated for 3 h at 37 °C, optical density (OD) was measured using an ELISA reader (Epoch, Biotek Instruments Inc., USA) at 570 nm. Cells cultured in a 24-well plate without specimens were saved for use as the negative control. Cell viability was calculated according to the following eq. (1):

$$\text{Viability rate (\%)} = \frac{OD_s - OD_b}{OD_n - OD_b} \times 100\% \quad (1)$$

where, s represents the measured OD of the specimens and n and b represent the measured optical densities of the negative control and the blank, respectively.

2.4. Statistical analysis

Statistical software (IBM SPSS Statistics, v19.0 version, USA) was applied for data analysis. After Kolmogorov–Smirnov goodness of fit and Levene's tests, Vickers hardness, contact angle and MTT assays were compared among groups using one-way analysis of variance with Bonferroni's post hoc test ($\alpha = 0.05$).

3. Results

3.1. Morphology features

The optical micrographs of the AS-TG and SHT specimens are depicted in Fig. 1. The apparently dendritic and interdendritic matrices without precipitates were observed in the AS-TG specimen, while the grain boundary was nearly indistinguishable, suggesting the presence of the one phase (Fig. 1(a)). Heat-treatment resulted in the recrystallization of grains in the specimens (Figs. 1(b) to 1(e)). The shapes and sizes of the grains were affected by the SHT temperature, revealing that the grain size increased approximately from 71 μm to 95 μm when the SHT temperature grow from 700 to 1000 $^{\circ}\text{C}$. Also, the needle-like intermetallics started to appear when SHT temperatures was above 900 $^{\circ}\text{C}$, as shown in Fig. 1(d) and 1(e), implying that α phase transformation occurred.

3.2. Microstructural variations

For further examination of the microstructural changes due to SHT, the SEM micrographs of the investigated specimens are shown in Fig. 2 and Fig. 3. The SHT-700 specimen exhibited a fine pseudo-dendrite morphology and clear grain boundaries (dotted black line), as shown in Fig. 2(a). Within the region shown by the black square, a high magnification of SEM micrograph, as shown in Fig. 2(b), showed the particle-like structures. The EDS analysis (Fig. 2(c)) indicated that the main chemical compositions were Ti and Ge. As SHT temperature increased to 900 $^{\circ}\text{C}$, structural morphologies dramatically re-arranged. The SHT-900 specimen presented a higher volume fraction of needle-like structures, as shown in Fig. 3(a), which consistent with OM observation. The needle-like structures accompanied with lath-like structures were formed in the SHT-1000 specimen, as shown in Fig. 3(b). While, it was found that the chemical compositions of both needle-like and lath-like structures in the SHT-1000 specimen were similar with the SHT-700

specimen.

Fig. 4 displays XRD spectra of the SHT specimens, as well as AS-TG. An α -hcp (hexagonal close-packed) structure was the only detectable phase in the AS-TG specimen, as shown in Fig. 4(a). Although peaks belonging to the α -Ti phase slightly shifted towards larger angle after SHT, no additional peaks no additional peaks were observed in the SHT specimens, as shown in Figs. 4(b) to 4(e), indicating that a remarkable phase transformation could not be distinguished. However, the α and α' phases probably possess similar X-ray diffractograms and show the diffraction peaks at the same two-theta values. Accordingly, TEM bright-field micrographs and selective area diffraction patterns (SADPs) were performed to further identify in detail (Fig. 5). Fig. 5(a) demonstrated large grains with several dislocations in the α -matrix of the SHT-700 specimen due to the casting procedure. The inserted SADP perpendicular to [0001] of zone A exhibited the α -hcp structure without extra diffraction spots, which consistent with results of the XRD pattern. Similar results were observed in the SHT-800 specimen. The TEM micrograph of the axial-section extracted from $[2\bar{1}\bar{1}0]$ of the SHT-900 specimen as shown in Fig. 5(b) revealed dislocations with high density mainly in form of dislocation tangles in the α -matrix. Additional acicular structures (denoted as zone B) were observed. The inserted SADP of zone B proved the extra diffraction spots with lower intensities were presented in the α -hcp structure, and identified as the α' -martensite phase according to the camera length and d -spacing of the super-lattice spots, meaning that phase transformation occurred when SHT temperature was above 900 $^{\circ}\text{C}$.

3.3. Material properties

Fig. 6 illustrates the Vickers microhardness of the SHT and AS-TG specimens, with cp-Ti serving as the control. The average hardness of the AS-TG specimen was 722.6 Hv, and with an increase in SHT temperature, the hardness of SHT specimens expectedly increased. The SHT-1000 specimen exhibited statistically higher hardness than AS-TG specimen ($p = 0.042$). Also, there were statistically differences in hardness between SHT-1000 and cp-Ti ($p = 0.002$), and SHT-900 and cp-Ti ($p = 0.017$). Fig. 7 shows the contact angles of the SHT and AS-TG specimens, with cp-Ti serving as the control. The AS-TG and cp-Ti specimens exhibited no statistical difference in contact angle. Notably, heat treatment resulted in a dramatic increase in the contact angle of the specimens. The SHT-700 specimen possessed the highest contact angles among groups (all $p < 0.001$). While, with an increase in SHT

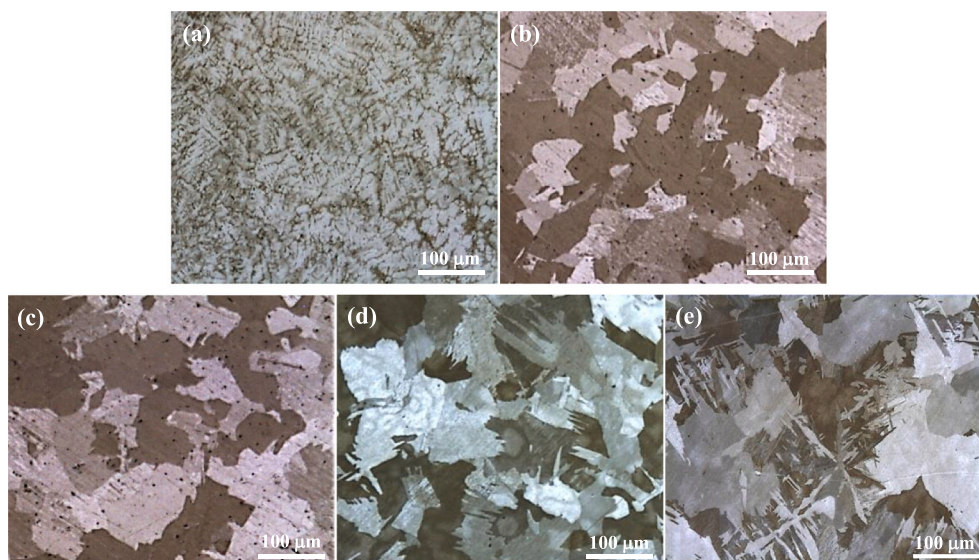


Fig. 1. OM micrographs of the (a) AS-TG, (b) SHT-700, (c) SHT-800, (d) SHT-900, and (e) SHT-1000 specimens.

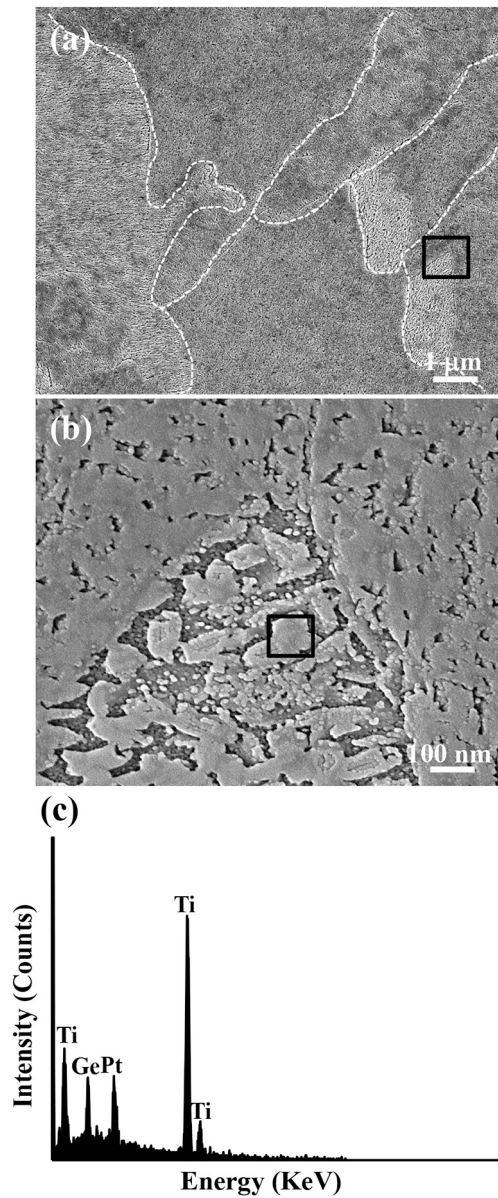


Fig. 2. SEM micrographs of the (a) SHT-700, (b) a high magnification taken from the black square of (a), and (c) EDS spectrum taken from the black square of (b) (The Pt element was generated from the thin film coating of Pt for providing electrical conductivity and preventing specimen charging effects in the SEM).

temperature, the contact angles of SHT specimens decreased. There were no statistical differences in contact angle among the SHT-900, SHT-1000, and cp-Ti specimens.

3.4. Cell response and adhesion behavior

MTT assay results for MG-63 and NIH-3T3 cultured in the SHT and AS-TG specimens, with cp-Ti serving as the control, are shown in Fig. 8. After 8 h of incubation, the relative viabilities of all groups were above 70% for both MG-63 and NIH-3 T3, indicating that the SHT and AS-TG specimens are nontoxic. The relative viabilities increased with incubation time, indicating that cell proliferation for all groups was statistically enhanced. For MG-63 cell, although the viability rate of the AS-TG specimen was slightly lower than those of cp-Ti specimen, there was no statistical difference at each time point. The SHT did not enhance the relative viabilities at low temperature. However, when the SHT

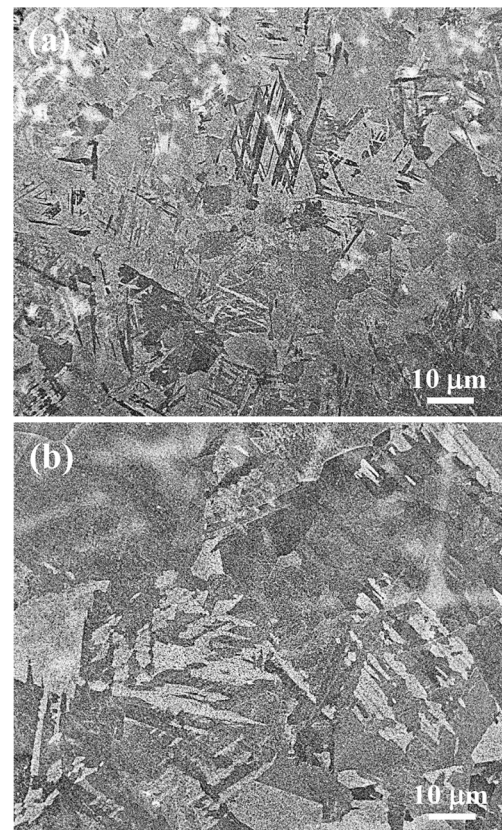


Fig. 3. SEM micrographs of (a) SHT-900 and (b) SHT-1000 specimens.

temperature was above 900 °C, the SHT-900 and SHT-1000 specimens exhibited the highest viability rates among groups at each time point, as shown in Fig. 8(a). Similar results of the viability rates were observed for NIH-3T3, as shown in Fig. 8(b). Fig. 9 presents SEM micrographs of cell morphology from the SHT-900 specimen after 72 h of incubation with MG-63 (Fig. 9(a)) and NIH-3T3 (Fig. 9(b)), showing good adhesion and differentiation with flattened morphology and numerous filopodia. A similar feature could also be found in the SHT-1000 specimen.

4. Discussion

Lin et al. [19] have demonstrated that the AS-TG alloy exhibited excellent mechanical properties, such as high yield strength, and ultimate tensile strength and elongation, high yield strength, ultimate tensile strength and elongation, and was considered potential dental material. Hence, the AS-TG alloy was further selected to investigate the effect of solution heat-treatment temperatures on the microstructure transformation and biocompatibility. It is well known that the formation of α' -martensitic phase depended on the heat-treatment temperature in the Ti-based alloys. In the present study, XRD and TEM analysis results demonstrated that the AS-TG specimen or SHT at lower temperature specimen (such as SHT-700 and SHT-800) was an essential α -hcp structure [19]. Nevertheless, when the SHT temperature was above 900 °C, the specimen contained a mixture of α and α' phases without any precipitated particles, suggesting that temperature was sufficient to trigger α' phase formation. According to this finding, it is clearly seen that the SHT with a higher temperature enhanced the hardness of the AS-TG alloy as compared with the heat-treated control cp-Ti (Fig. 6), revealing that the phase transformation from α to ($\alpha + \alpha'$) resulted in AS-TG alloy hardening. This feature can be attributed that the formation of α' -martensitic phase can promote the mechanical properties (such as strength, hardness, and wear resistance) of Ti alloys [2,4,6–8].

Biocompatibility is a critical issue in developing new Ti-based alloys

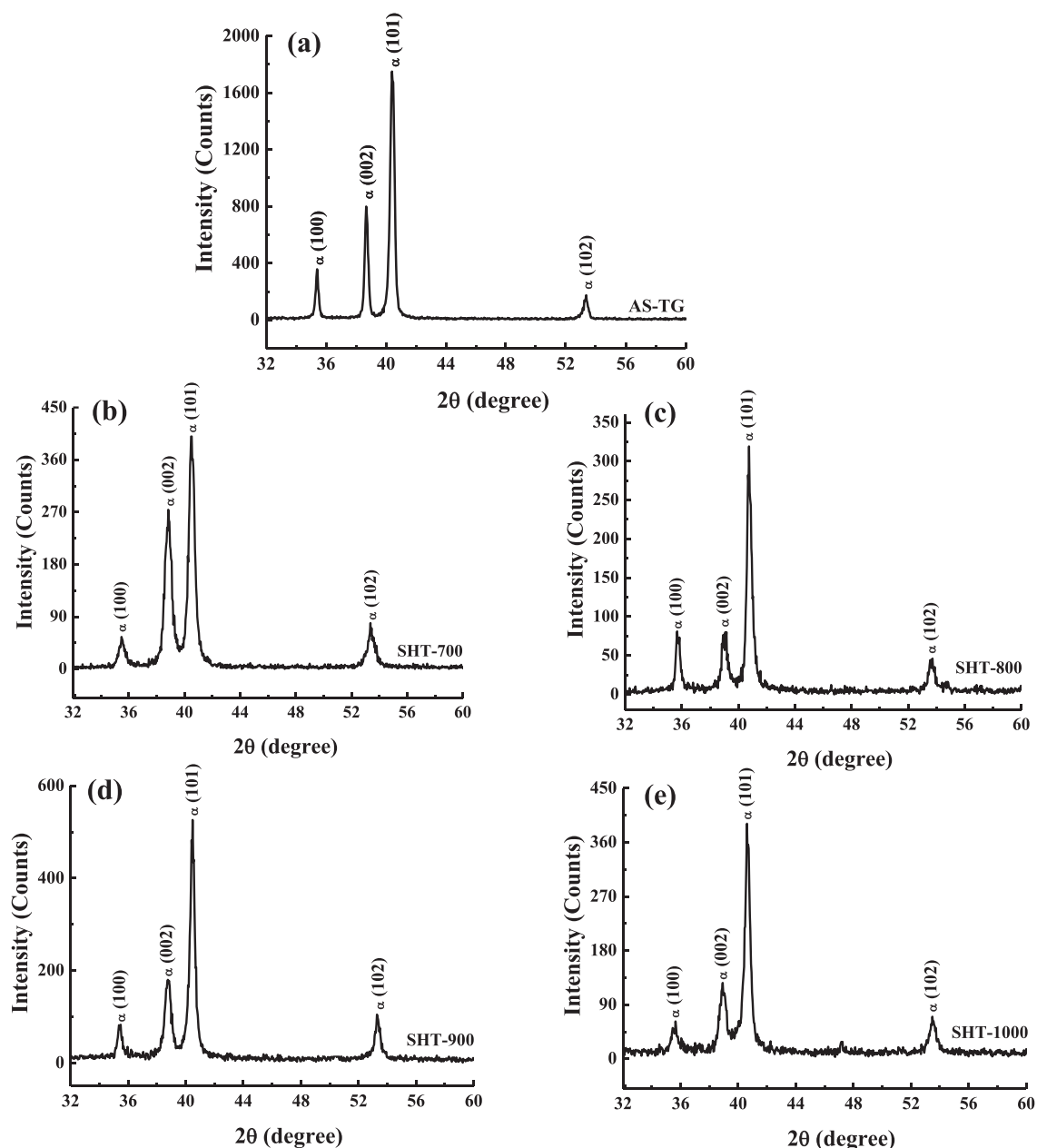


Fig. 4. XRD patterns of (a) AS-TG, (b) SHT-700, (c) SHT-800, (d) SHT-900, and (e) SHT-1000 specimens.

for implanted biomaterials. A suitable surface topography influences cellular responses, including cell proliferation, differentiation, and the production of local growth factors and cytokines [22–24]. Hence, variations in the surface topography have attracted considerable attention for moderating cellular responses [25]. The wettability, largely dependent on surface energy, is another determining surface property for protein adsorption, and consequently, for cell attachment and proliferation [24,26]. More recent studies focused on the simultaneous effects of both surface topography and wettability on cellular behaviors. It is not easy to separate the effects of surface wettability from those of other surface characteristics [27]. Moreover, increased wettability, which efficiently modulates osteoblast maturation and differentiation, was considered desirable for Ti implants due to the enhancement of interactions between implant surfaces and the biologic environment [28]. With higher surface energy, cell adhesion and spreading and the rate and extent of bone formation increased. Theoretically, pure Ti surfaces exhibit hydrophilic properties due to the spontaneous growth of an

oxide layer, which is essential for forming calcium phosphate layers and osseointegration. Ti surfaces exhibit increased hydrophobicity resulting from the high absorption tendency of inorganic anions or organic hydrocarbon contaminants from the atmosphere. In this study, the AS-TG specimens exhibited similar wettability to cp-Ti. SHT decreased the wettability of the SHT-700 and SHT-800 specimens, which presumably decelerated primary interactions of cellular attachment and proliferation [29], which was confirmed by the present MTT assay. With an increase in the treatment temperature, results showed that the AS-TG specimen shifted from hydrophobic to hydrophilic. The morphology and phase for the SHT-900 and SHT-1000 specimens differed from those of investigated specimens, which may affect the wettability, and the formation of α' phase may be well hydrophilic.

A variety of cell lines from humans and animals were used to evaluate the biocompatibility of the new biomaterials. The periodontium comprises four different tissues, including the root cementum, alveolar bone, gum, and periodontal ligament [30]. Two kinds of cell lines,

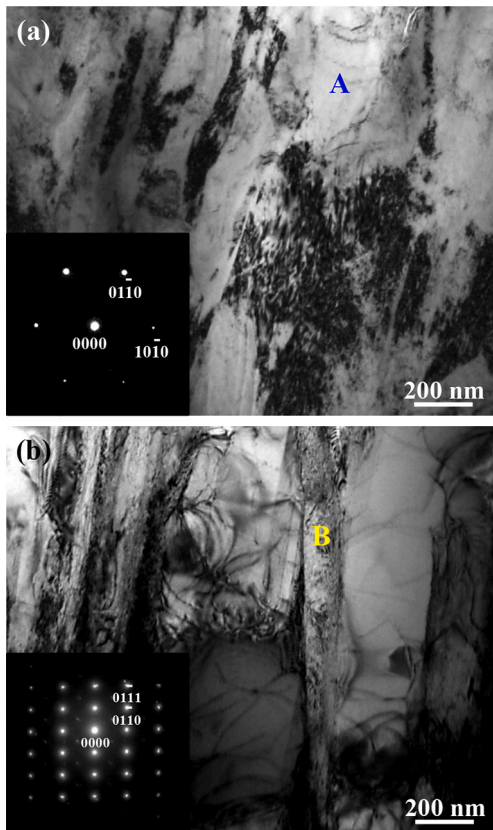


Fig. 5. TEM bright-field images and corresponding SADPs (inset) of the (a) SHT-700 and (b) SHT-900 specimens.

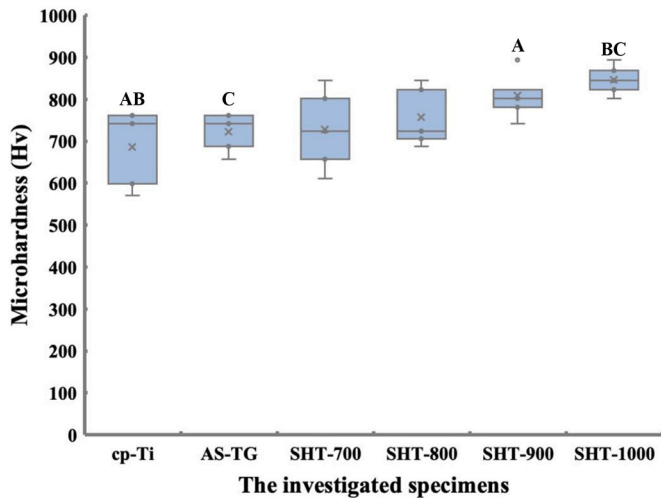


Fig. 6. Microhardness of the investigated specimens. The same capital letter indicates static difference between groups.

osteoblast-like MG-63 and NIH-3T3 fibroblast cells were used to evaluate cellular interactions in the present study due to simple manipulation and high employability. Cell recruitment and proliferation increased with an increasing incubation time for both MG-63 and NIH-3T3 cells, confirming that AS-TG and heat-treated AS-TG specimens supported cell attachment and proliferation. Generally, cells attached more rapidly onto the SHT-1000, followed by the cp-Ti and AS-TG specimens for both cell types. The results obtained followed the trend reported by a previous study in which surfaces with hydrophilic properties induced higher cell adhesion and proliferation than those with

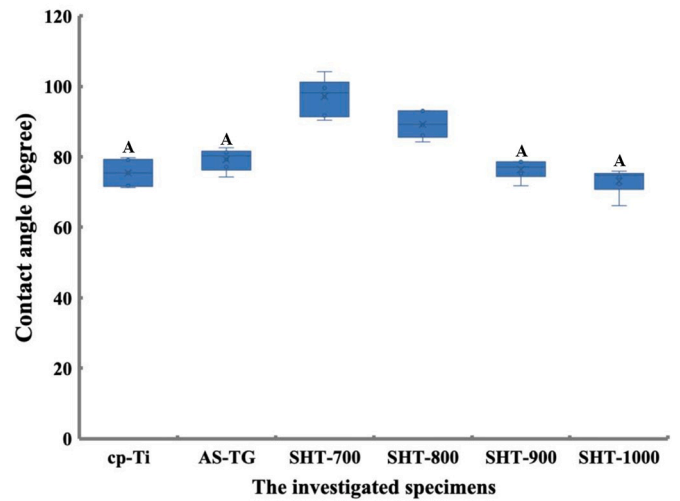


Fig. 7. Contact angle of the investigated specimens. The same capital letter indicates no static difference among groups.

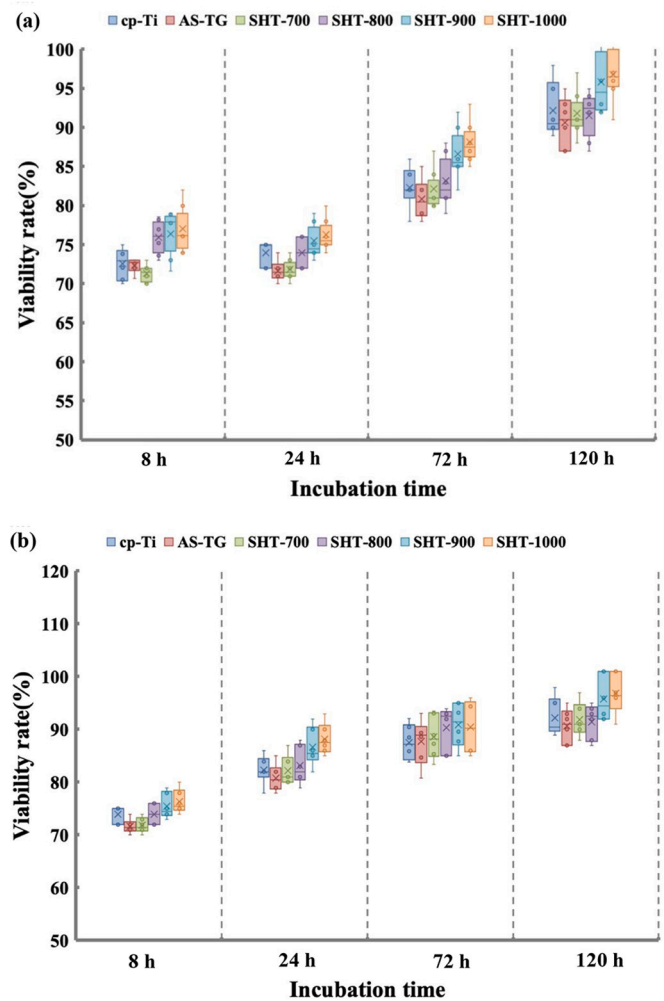


Fig. 8. MTT assay results showing (a) MG-63 and (b) NIH-3T3 viability after incubation in the AS-TG and SHT specimens, with cp-Ti serving as the control.

hydrophobic properties [31]. These results may also be attributed to the effect of α' phase formation on the SHT-1000 specimen, which produced higher reactivity. Accordingly, it is believed that the formation of α'

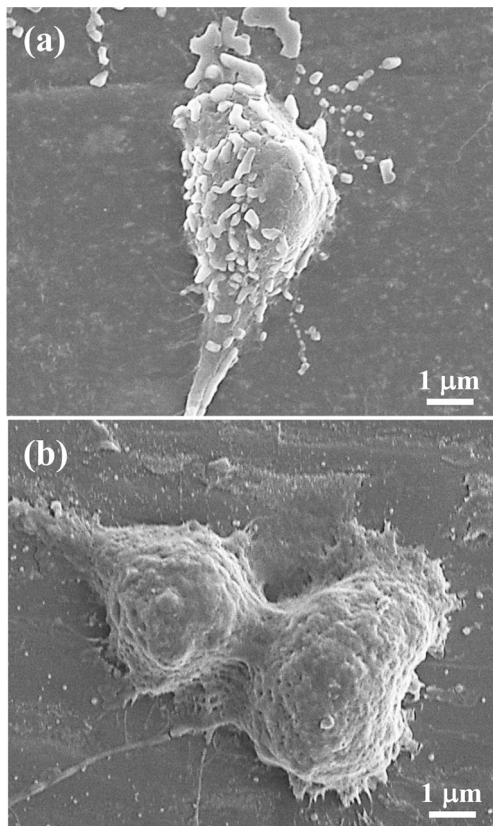


Fig. 9. SEM micrographs of cell morphology after 72 h incubation on the SHT-900 specimen with (a) MG-63 and (b) NIH-3T3 cells.

phase not only increased the hardness, but also enhanced the wettability of the AS-TG alloy. Finally, further studies should be conducted to validate the present findings.

5. Conclusions

The microstructure of the AS-TG could be altered through different SHT temperatures. As the SHT temperature increased to 900 °C, the crystallographic phase of the AS-TG alloy transformed from α to $(\alpha + \alpha')$. The microhardness and wettability also improved after SHT above 900 °C. The SHT-1000 specimen exhibited the highest cell viability, which was even more significant than cp-Ti. This result indicated that the cell response and adhesion behavior of the AS-TG alloy are related to the microstructures and phase transformation. Therefore, the findings of the present study could provide useful scientific information in the improvement of Ti–Ge alloy.

Funding

This research received no specific grant from any funding agency in the public, commercial, or not-for-profit sectors.

Ethical approval

This article does not contain any studies with human participants or animals performed by any of the authors.

Informed consent

For this type of study, formal consent is not required.

Data availability

The raw/processed data required to reproduce these findings cannot be shared at this time due to technical or time limitations.

Declaration of Competing Interest

All authors declare no conflicts of interest.

References

- [1] T. Nagase, Y. Iijima, A. Matsugaki, K. Ameyama, T. Nakano, Design and fabrication of Ti–Zr–Hf–Cr–Mo and Ti–Zr–Hf–co–Cr–Mo high-entropy alloys as metallic biomaterials, *Mater. Sci. Eng. C* 107 (2020) 110322.
- [2] J. Jiang, C. Zhou, Y. Zhao, F. He, X. Wang, Development and properties of dental Ti–Zr binary alloys, *J. Mech. Behav. Biomed. Mater.* 112 (2020) 104048.
- [3] J.D.C. Tardelli, M.L. da Costa Valente, T.T. de Oliveira, A.C. Dos Reis, Influence of chemical composition on cell viability on titanium surfaces: a systematic review, *J. Prosthet. Dent.* 125 (2020) 421–425.
- [4] I. Cvijović-Alagić, N. Gubelj, M. Rakin, Z. Cvijović, K. Gerić, Microstructural morphology effects on fracture resistance and crack tip strain distribution in Ti–6Al–4V alloy for orthopedic implants, *Mater. Des.* 53 (2014) 870–880.
- [5] M.G. de Mello, C.F. Salvador, A. Cremasco, R. Caram, The effect of Sn addition on phase stability and phase evolution during aging heat treatment in Ti–Mo alloys employed as biomaterials, *Mater. Charact.* 110 (2015) 5–13.
- [6] H.-C. Hsu, S.-C. Wu, S.-K. Hsu, C.-T. Li, W.-F. Ho, Effects of chromium addition on structure and mechanical properties of Ti–5Mo alloy, *Mater. Des.* 65 (2015) 700–706.
- [7] X. Liu, S. Chen, J.K. Tsoi, J.P. Matinlinna, Binary titanium alloys as dental implant materials—a review, *Regenerative Biomaterials* 4 (2017) 315–323.
- [8] J.W. Nicholson, Titanium alloys for dental implants: a review, *Prosthesis* 2 (2020) 100–116.
- [9] J. Jiang, Y. Zhao, X. Wang, Effects of Zr addition on the deformation behavior, microstructure and mechanical properties of dental Ti alloys, *Mater. Sci. Eng. A* 794 (2020) 139808.
- [10] H.-C. Hsu, S.-C. Wu, Y.-S. Hong, W.-F. Ho, Mechanical properties and deformation behavior of as-cast Ti–Sn alloys, *J. Alloys Compd.* 479 (2009) 390–394.
- [11] P.C.-H. Kuo, H.-H. Chou, Y.-H. Lin, P.-W. Peng, K.-L. Ou, W.-R. Lee, Effects of surface functionalization on the nanostructure and biomechanical properties of binary titanium–niobium alloys, *J. Electrochem. Soc.* 159 (2012) E103–E107.
- [12] J. Wang, Y. Liu, P. Qin, S. Liang, T. Sercombe, L. Zhang, Selective laser melting of Ti–35Nb composite from elemental powder mixture: microstructure, mechanical behavior and corrosion behavior, *Mater. Sci. Eng. A* 760 (2019) 214–224.
- [13] W. Chen, C. Chen, X. Zi, X. Cheng, X. Zhang, Y.C. Lin, K. Zhou, Controlling the microstructure and mechanical properties of a metastable β titanium alloy by selective laser melting, *Mater. Sci. Eng. A* 726 (2018) 240–250.
- [14] H. Dong, Z. Feng, S. Liang, X. Sun, J. Li, D. Wu, R. Su, X. Zhang, Evolution of microstructure, mechanical properties and corrosion behaviors using cooling rate regulation in a novel ZrTi-based alloy, *Journal of Materials Research and Technology* 9 (2020) 3471–3480.
- [15] K. Qiu, W. Lin, F. Zhou, H. Nan, B. Wang, L. Li, J. Lin, Y. Zheng, Y. Liu, Ti–Ga binary alloys developed as potential dental materials, *Mater. Sci. Eng. C* 34 (2014) 474–483.
- [16] G. Gerber, A. Léonard, Mutagenicity, carcinogenicity and teratogenicity of germanium compounds, *Mutation Research/Reviews in Mutation Research* 387 (1997) 141–146.
- [17] T. Kitashima, K. Suresh, Y. Yamabe-Mitarai, Effect of germanium and silicon additions on the mechanical properties of a near- α titanium alloy, *Mater. Sci. Eng. A* 597 (2014) 212–218.
- [18] T.B. Massalski, H. Okamoto, P. Subramanian, L. Kacprzak, W.W. Scott, *Binary Alloy Phase Diagrams*, American Society for Metals Metals Park, OH, 1986.
- [19] W.J. Lin, B.L. Wang, K.J. Qiu, F.Y. Zhou, L. Li, J.P. Lin, Y.B. Wang, Y.F. Zheng, Ti–Ge binary alloy system developed as potential dental materials, *J. Biomed. Mater. Res. B Appl. Biomater.* 100 (2012) 2239–2250.
- [20] O. Vdovychenko, O. Ivanova, Y. Podrezov, M. Bulanova, I. Fartushna, Mechanical behavior of homogeneous and nearly homogeneous Ti3Sn: role of composition and microstructure, *Mater. Des.* 125 (2017) 26–34.
- [21] S. Miyazaki, H. Kim, H. Hosoda, Development and characterization of Ni-free Ti-base shape memory and superelastic alloys, *Mater. Sci. Eng. A* 438 (2006) 18–24.
- [22] S.-R. Ryoo, Y.-K. Kim, M.-H. Kim, D.-H. Min, Behaviors of NIH-3T3 fibroblasts on graphene/carbon nanotubes: proliferation, focal adhesion, and gene transfection studies, *ACS Nano* 4 (2010) 6587–6598.
- [23] J. Lee, B. Kang, B. Hicks, T.F. Chancellor, B.H. Chu, H.-T. Wang, B.G. Keselowsky, F. Ren, T.P. Lele, The control of cell adhesion and viability by zinc oxide nanorods, *Biomaterials* 29 (2008) 3743–3749.
- [24] J. Rosales-Leal, M. Rodríguez-Valverde, G. Mazzaglia, P. Ramon-Torregrosa, L. Diaz-Rodriguez, O. Garcia-Martinez, M. Vallecillo-Capilla, C. Ruiz, M. Cabrerizo-Vilchez, Effect of roughness, wettability and morphology of engineered titanium surfaces on osteoblast-like cell adhesion, *Colloids Surf. A Physicochem. Eng. Asp.* 365 (2010) 222–229.
- [25] D. Khang, J. Lu, C. Yao, K.M. Haberstroh, T.J. Webster, The role of nanometer and sub-micron surface features on vascular and bone cell adhesion on titanium, *Biomaterials* 29 (2008) 970–983.

- [26] Y. Zhang, O. Andrukhov, S. Berner, M. Matejka, M. Wieland, X. Rausch-Fan, A. Schedle, Osteogenic properties of hydrophilic and hydrophobic titanium surfaces evaluated with osteoblast-like cells (MG63) in coculture with human umbilical vein endothelial cells (HUVEC), *Dental Materials* 26 (2010) 1043–1051.
- [27] J. Barthes, M. Cazzola, C. Muller, C. Dollinger, C. Debry, S. Ferraris, S. Spriano, N. E. Vrana, Controlling porous titanium/soft tissue interactions with an innovative surface chemical treatment: responses of macrophages and fibroblasts, *Mater. Sci. Eng. C* 112 (2020) 110845.
- [28] F. Bartolomeu, N. Dourado, F. Pereira, N. Alves, G. Miranda, F. Silva, Additive manufactured porous biomaterials targeting orthopedic implants: a suitable combination of mechanical, physical and topological properties, *Mater. Sci. Eng. C* 107 (2020) 110342.
- [29] A. Toffoli, L. Parisi, M.G. Bianchi, S. Lumetti, O. Bussolati, G.M. Macaluso, Thermal treatment to increase titanium wettability induces selective proteins adsorption from blood serum thus affecting osteoblasts adhesion, *Mater. Sci. Eng. C* 107 (2020) 110250.
- [30] R. Osorio, C.A. Alfonso-Rodríguez, E. Osorio, A.L. Medina-Castillo, M. Alaminos, M. Toledano-Osorio, M. Toledano, Novel potential scaffold for periodontal tissue engineering, *Clin. Oral Investig.* 21 (2017) 2695–2707.
- [31] M. Arciniegas, J. Pena, F.J. Gil, J.M. Manero, In vitro response of preosteoblastic MG63 cells on Ni-free Ti shape memory substrates, *J Biomed Mater Res B Appl Biomater* 101 (2013) 709–720.